Asian Journal of Chemistry; Vol. 37, No. 12 (2025), 3001-3010
ASIAN JOURNAL OF CHEMISTRY
https://doi.org/10.14233/ajchem.2025.34632

ROS-Responsive Drug Release from Green Synthesized Silver Nanoparticles Loaded Saponin Nanoarchitectures for Targeted Cancer Therapy

SUBRAMANIAM KRISHNAVENI[1], KALYANASUNDARAM PARVATHI[1,*] and SRINIVASAN AYYANAAR[2,*]

[1]PG & Research Department of Chemistry, L.R.G. Government Arts College for Women, Tiruppur-641604, India
[2]Department of Biotechnology, Kalaignarkarunanidhi Institute of Technology, Coimbatore-641402, India

*Corresponding authors: E-mail: pkrparvathi@gmail.com; s.ayyanaar@gmail.com

Received: 5 August 2025 *Accepted*: 30 September 2025 *Published online*: 30 November 2025 AJC-22188

Curcumin (CUR), a bioactive polyphenol derived from turmeric, has gained attention in drug delivery systems due to its potent anti-inflammatory, antioxidant and anticancer properties. It can inhibit cancer cell proliferation, metastasis and angiogenesis, while also sensitizing tumor cells to chemotherapy and overcoming drug resistance making it a strong candidate as an adjuvant in cancer therapy. However, curcumin's clinical translation is hindered by poor bioavailability and rapid metabolism. To address these challenges, a reactive oxygen species (ROS)-responsive nanoparticle system is developed based on green synthesized silver nanoparticles (AgNPs). The AgNPs were fabricated using *Phyllanthus niruri* leaves extract, serving as both a reducing and capping agent. These biogenic AgNPs were embedded in a saponin (SA) matrix chosen for its ROS-sensitivity due to lipid peroxidation at the double bonds further reinforced with starch and loaded with CUR, resulting in a multifunctional nanocomposite, Ag@SA-Starch-CUR-NPs. This platform leverages the tumor microenvironments acidic pH and elevated ROS levels to trigger targeted drug release. Saponin undergoes oxidative degradation in response to ROS, while starch enhances pH-sensitive CUR release under acidic conditions. The nanocomposites demonstrated high encapsulation efficiency (89.50%), pH and ROS-responsive release kinetics, particularly favouring drug release in tumor-like conditions. Physico-chemical characterization confirmed the composites thermal stability, spherical morphology and uniform elemental distribution. *In vitro* assays on MCF-7 breast cancer cell lines revealed potent cytotoxic activity ($IC_{50} \approx 19.5 \pm 0.20$ µg/mL), while anti-inflammatory testing showed significant activity ($IC_{50} = 20.13$ µg/mL), outperforming the standard formulations. Collectively, these findings highlight Ag@SA-Starch-CUR-NPs as a promising, biocompatible and environmentally friendly nanoplatform for targeted cancer therapy, offering improved drug delivery performance and therapeutic outcomes.

Keywords: Silver nanoparticles, Saponin, Curcumin, ROS responsive, Cytotoxicity.

INTRODUCTION

Reactive oxygen species (ROS) are highly reactive molecules, including superoxide (O_2^-), hydroxyl radical ($^{\bullet}OH$) and hydrogen peroxide (H_2O_2), mainly produced in mitochondria and the endoplasmic reticulum. At normal levels, ROS help regulate cell signaling, immune defense and other physiological processes [1,2]. However, excessive ROS can cause oxidative stress, damaging DNA, proteins and lipids, which may lead to cell death and contribute to diseases like cancer, cardiovascular disorders and neurodegenerative conditions [3-5]. Nanotechnology involves manipulating materials at the nanoscale (1-100 nm), where they exhibit unique properties unlike their bulk forms. Silver nanoparticles (AgNPs) are widely studied due to their high surface area, strong antimicrobial activity and excellent electrical and thermal conductivity. These features make AgNPs highly suitable for applications in drug delivery, biosensing, electronics and water purification [6-9].

Recently, biogenic materials such as bacteria, fungi, algae, viruses and plant extracts have been used for green nanoparticle synthesis [10-12]. Among them, plant-based synthesis is faster and more stable due to phytochemicals (*e.g.* alkaloids, terpenoids, tannins, polyphenols) that act as natural reducing and stabilizing agents. *Phyllanthus niruri* (commonly known as Chanca Piedra) is a tropical coastal plant rich in bioactive compounds such as flavonoids, lignans, alkaloids, terpenoids, polyphenols, tannins, coumarins and saponins, which contribute to its notable medicinal and pharmacological properties [13,14].

Saponin (SA) are naturally occurring compounds widely distributed in the plant kingdom. Their amphiphilic structure imparts high surface activity and self-assembly properties, making them effective natural biosurfactants [15]. These characteristics have positioned saponins as promising candidates for drug delivery system (DDS) applications. Numerous studies report enhanced solubility and bioavailability of drugs when combined with saponins, likely due to synergistic interactions [16,17]. This highlights their potential not only as functional adjuvants but also as novel carrier materials in DDS design. Similarly, curcumin, a polyphenolic compound from the ginger family, has antioxidant, anti-inflammatory, anticancer and anti-aging properties [18]. However, its poor stability, low solubility and limited bioavailability hinder its use in food and drug formulations [19]. To overcome these issues, biocompatible nanoparticles made from natural polymers like proteins and polysaccharides are used to encapsulate and deliver curcumin [20-23]. These systems enhance its stability, solubility and controlled release, improving its effectiveness.

In recent years, biopolymers such as chitosan (CS), polyethylene glycol (PEG), polylactic acid (PLA), polyvinyl alcohol (PVA) and starch have been extensively employed in biomedical applications due to their excellent biodegradability within the biological systems [24]. Among them, starch has emerged as a promising bioactive and biocompatible material for various biomedical uses, particularly in controlled drug delivery. As a naturally abundant polysaccharide, starch is hydrophilic, biodegradable, non-toxic and cost-effective. These characteristics make it highly suitable for nanoparticle-based drug delivery systems. Starch nanoparticles, typically ranging from 10 to 1000 nm, have shown significant potential as nanocarriers for controlled and targeted drug release applications [20,25-27].

This research aims to advance the understanding of reactive oxygen species (ROS)-based drug delivery systems and contribute to the development of novel nanotherapeutics with improved clinical efficacy. The present study investigates the comparative roles of green synthesized silver nanoparticles (AgNPs), using *Phyllanthus niruri* extract as both a capping and reducing agent. These AgNPs were incorporated into a ROS-sensitive saponin (SA) matrix, further combined with starch and loaded with curcumin (CUR) to form a composite nanoparticle system (Ag@SA-Starch-CUR-NPs). This study provides a comprehensive analysis of the synthesis, characterization and biomedical applications of the developed nanocomposite. The Ag@SA-Starch-CUR-NPs demonstrated significant anti-inflammatory properties and *in vitro* cytotoxicity against human breast cancer (MCF-7) cells, along with morphological evidence supporting their potential as multifunctional agents. This work also emphasizes the future prospects of Ag@SA-Starch-CUR-NPs in biomedicine, particularly in drug delivery, metabolic transport and therapeutic applications.

EXPERIMENTAL

Phyllanthus niruri plants were collected from the vicinity of Tiruppur city, India (coordinates: 11.1085º N, 77.3411º E). Silver nitrate ($AgNO_3$) and saponin (SA) were procured from Alfa Aesar, whereas starch and curcumin (CUR) were obtained from Sigma-Aldrich. Milli-Q water was used for the preparation of all solutions. The analytical-grade organic solvents were used without further purification.

Extract preparation of *P. niruri* plant: The leaves were shade-dried for 24 h at 70 ºC and ground into a fine powder. About 10 g of powder was added to 100 mL of sterilized, filtered water and stirred thoroughly. The resulting mixture was first filtered through Whatman No. 1 filter paper (Maidstone, UK), followed by a 0.22 µm membrane filter (Millipore) to obtain a clear aqueous extract. The extract was then centrifuged at 10,000 rpm for 5 min to remove heavy biomaterials. The supernatant, containing the bioactive components, was stored at 4 ºC for further use.

Synthesis of AgNPs using *P. niruri* leaves extract: In brief, 10 mL of aqueous *P. niruri* leaves extract was mixed with 100 mL of 1 mM $AgNO_3$ solution and incubated at 50 ºC for 5 h until a brown precipitate formed. The precipitate was centrifuged at 3000 rpm for 15 min and the resulting pellet was dried on a glass plate in an oven at 45 ºC for 24-48 h. The dried material was then ground into a fine powder using a mortar and pestle.

Synthesis of Ag@SA-NPs: The green synthesized AgNPs were surface-modified using 3 mL of SA *via* a simple stirring method at room temperature for 25 min to ensure complete coating. After cooling to ambient temperature, the resulting SA-coated AgNPs dispersion was separated and thoroughly washed with acetone and double-distilled water to eliminate any residual impurities. Finally, the purified SA-coated AgNPs (Ag@SA-NPs) were vacuum dried at room temperature for 4 h.

Synthesis of Ag@SA-Starch-CUR-NPs: The Ag@SA-Starch-CUR-NPs were synthesized using an *in situ* filling method, as illustrated in Fig. 1. Initially, 100 mg of dried Ag @SA-NPs with an oil-based surface were dispersed and mixed with 3 mL of starch solution under continuous stirring for 1 h. Subsequently, 3 mL of an aqueous CUR solution was added. To facilitate electrostatic interactions between the negatively charged CUR and the positively charged starch molecules adsorbed on the Ag@SA-NPs surface, the mixture was gently shaken at room temperature for 7 h. The resulting suspension was then magnetically separated and washed with distilled water by centrifugation at 5000 rpm for 10 min to remove unbound CUR. Finally, the purified Ag@SA-Starch-CUR-NPs were collected and dried into powder form for further analysis.

Characterization of Ag@SA-Starch-CUR-NPs: The reduction mechanism of green synthesized AgNPs was monitored using a Perkin-Elmer UV-Vis spectrophotometer over a range of 300-900 nm. XRD analysis using Cu*K*α radiation (λ = 1.5406 Å) on a D/Max-IIIC diffractometer confirmed the crystalline structures of AgNPs and Ag@SA-Starch-CUR-NPs by comparison with JCPDS data. FTIR spectra were recorded using an Avatar 360 spectrophotometer to identify functional groups in AgNPs, Ag@SA-NPs, starch, CUR and Ag@SA-Starch-CUR-NPs. SEM and TEM (Philips CM12, 120 kV) were used to examine surface and internal morphologies, respectively. TGA (Pyris 1) assessed thermal stability, while DLS analysis (Zetasizer, 660 nm) determined the hydrodynamic particle size at 25 ºC with a 90º scattering angle.

Determination of drug encapsulation efficiency: The CUR content encapsulated within the Ag@SA-Starch-CUR-

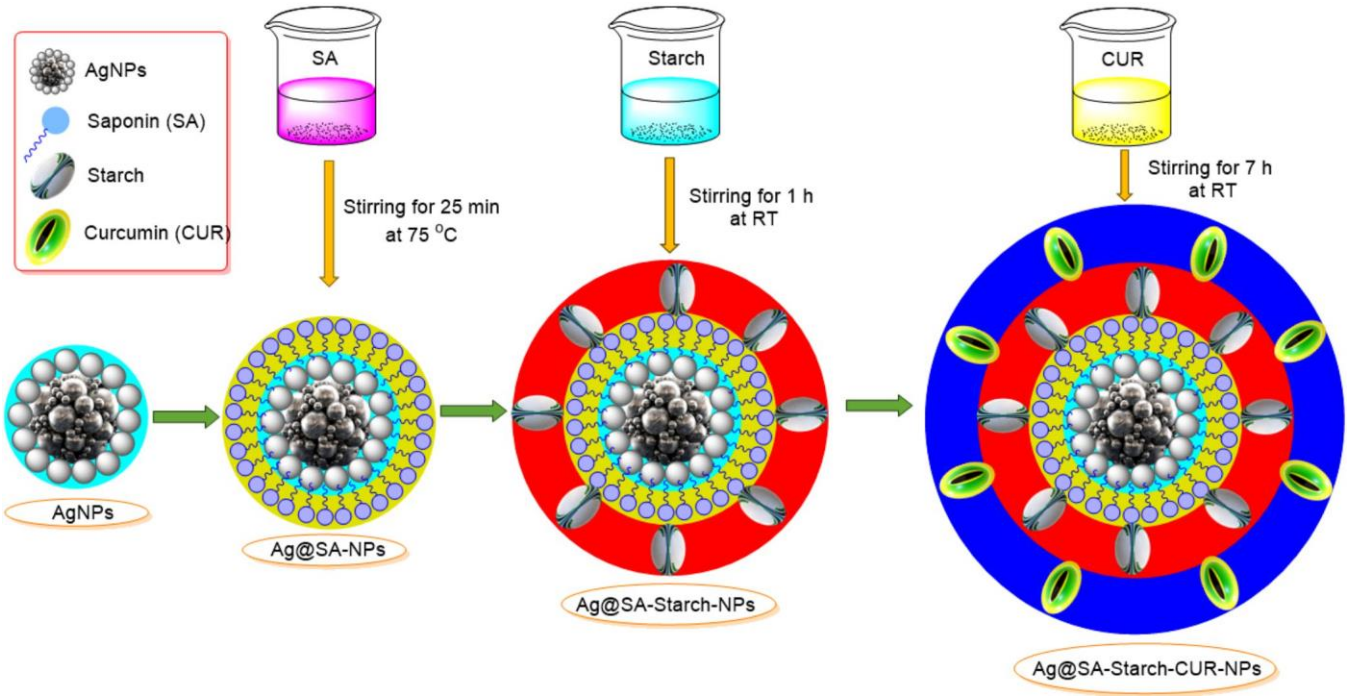

Fig. 1. Schematic drawing of AgNPs using *Phyllanthus niruri* leaves extract

NPs was determined by dissolving the nanoparticles in dichloromethane (DCM) and analyzing their UV-Vis absorption characteristics. Approximately 10 mg of Ag@SA-Starch-CUR-NPs were dissolved in 1 mL of DCM in a sealed glass tube, followed by the addition of 10 mL of phosphate buffer (pH 7.4). The mixture was magnetically stirred at room temperature for 2 h to facilitate the extraction of CUR. After complete evaporation of DCM, the solution was centrifuged at 5000 rpm for 10 min to separate the aqueous phase [28]. The concentration of CUR in buffer was quantified using a standard calibration curve based on its characteristic absorption peak at 421 nm. The drug content and encapsulation efficiency were calculated using the following equations:

$$\text{Drug content (\%)} = \frac{\text{Total amount of drug added} - \text{Free drug}}{\text{Total amount of drug added}} \times 100$$

$$\text{Encapsulation efficiency (\%)} = \frac{\text{Total amount of drug added} - \text{Free drug}}{\text{Wight of nanoparticles}} \times 100$$

***In vitro* drug release studies:** The *in vitro* release of CUR from Ag@SA-Starch-CUR-NPs was evaluated using a dialysis method. Approximately 100 mg of nanoparticles were placed into dialysis tubing (MWCO: 10 kDa) and immersed in 10 mL of phosphate buffer (pH 7.4 or 5.2) at 37 ºC with continuous shaking in dark [20]. At predetermined time intervals, 1.0 mL of release medium was withdrawn and replaced with an equal volume of fresh buffer to maintain sink conditions. The amount of CUR released was quantified using UV-Vis spectrophotometry at 421 nm. The drug release efficiency of Ag@SA-Starch-CUR-NPs was subsequently determined as follows:

$$\text{Drug releasing efficiency (\%)} = \frac{C_r}{C_o - C_t} \times 100$$

where C_r is the concentration of CUR released from Ag@SA-Starch-CUR-NPs at time t; C_o is the initial concentration of CUR encapsulated in Ag@SA-Starch-CUR-NPs.

***In vitro* anti-inflammatory assay:** The human red blood cell (HRBC) membrane stabilization assay was employed to assess the potential anti-inflammatory activity of Ag@SA-NPs and Ag@SA-Starch-CUR-NPs. Blood samples were collected from healthy volunteers who had abstained from non-steroidal anti-inflammatory drugs (NSAIDs) for at least two weeks. The samples were treated with Alsever's solution and centrifuged at 5000 rpm for 10 min to isolate RBCs. After washing with isosaline, the RBCs were exposed to varying concentrations of Ag@SA-Starch-CUR-NPs (20, 40, 60, 80 and 100 μg/mL). The mixtures, containing hyposaline, phosphate buffer and HRBC suspension, were incubated and then centrifuged at 3000 rpm for 5 min. Hemoglobin release was measured spectrophotometrically at 560 nm. Green synthesized diclofenac served as the standard, while Ag@SA-NPs were used as the control [29].

In vitro cytotoxicity studies

Cancer cell line culture: Human breast cancer cells (MCF-7) were cultured in Dulbecco's Modified Eagle Medium/ Nutrient Mixture F-12 (DMEM/F-12), supplemented with 100 μg/mL streptomycin, 100 μg/mL penicillin G, 2.5 μg/mL amphotericin B and 10% fetal bovine serum (FBS). Cells were seeded into 96-well culture plates and maintained until reaching confluence. Incubation was performed at 37 ºC in a humidified atmosphere containing 5% CO_2 in a CO_2 incubator.

MTT cytotoxic assay: The cytotoxicity of green synthesized AgNPs, Ag@SA-NPs and Ag@SA-Starch-CUR-NPs against MCF-7 breast cancer cells was evaluated using the MTT assay, following a previously established protocol [30]. Briefly, MCF-7 cells were seeded at a density of 1×10^4 cells per well in a 96-well plate and incubated for 24 h. After the initial incubation, the culture medium was replaced with 200 μL of fresh medium containing varying concentrations of the

test nanoparticles. Following another 24 h incubation, 20 µL of MTT solution (5 mg/mL in phosphate-buffered saline) was added to each well. The plates were wrapped in aluminum foil and incubated for an additional 4 h at 37 ºC. Thereafter, 100 µL of DMSO was added to each well to solubilize the purple formazan crystals formed by viable cells. Absorbance was measured at 570 nm with a reference wavelength of 630 nm using a 96-well plate reader. The half-maximal inhibitory concentration (IC_{50}) values (in µg/mL) for each nanoparticle type were calculated from triplicate experiments by plotting cell viability percentages against nanoparticle concentrations.

Acridine orange/ethidium bromide (AO/EB) staining assay: To assess nanoparticle-induced apoptosis, the morphological changes in MCF-7 cancer cells were evaluated using the acridine orange/ethidium bromide (AO/EB) double staining method. Cells were treated with green synthesized AgNPs, Ag@SA-NPs and Ag@SA-Starch-CUR-NPs at a fixed concentration of 5 µg/mL for 24 h. After treatment, 1 µg/mL of AO was added to each well and the cells were incubated in dark at 37 ºC for 15 min. Subsequently, ethidium bromide (EB) staining was performed, followed by thorough washing with phosphate-buffered saline to remove excess dye. The stained cells were examined using a Nikon Eclipse™ fluorescence microscope (Nikon & Co., Japan). Live, apoptotic and necrotic cells were distinguished based on characteristic fluorescence emission patterns: viable cells appeared green, early apoptotic cells showed green fluorescence with condensed or fragmented chromatin and late apoptotic or necrotic cells fluoresced orange to red due to EB uptake.

Statistical analysis: Experiments were performed in triplicate to ensure reliability. Data were analyzed using OriginPro 8.1 with one-way ANOVA and Tukey's test. Results are expressed as mean ± SEM (n = 3) and $p < 0.05$ was considered statistically significant.

RESULTS AND DISCUSSION

UV-Vis analysis: The UV-Vis spectra of the green synthesized AgNPs were recorded in the range of 300-900 nm. The characteristic surface plasmon resonance (SPR) peak for AgNPs was observed broadly around 425 nm, indicating successful nanoparticle formation. *P. niruri* leaves extract exhibited a distinct absorption peak near 340 nm. Upon synthesis, a redshift to 425 nm was noted, confirming the formation of AgNPs. The broadness of the peak from 425 to 450 nm suggests effective capping and stabilization of the nanoparticles by phytoconstituents from the plant extract (Fig. 2) [31]. This SPR band in the visible region also indicates that the synthesized AgNPs are active under the visible light.

FT-IR spectrum: The functional groups present in the green synthesized AgNPs, Ag@SA-NPs, starch, curcumin and Ag@SA-Starch-CUR-NPs were identified using FT-IR spectroscopy (Fig. 3). For the green synthesized AgNPs, a broad absorption band at 3350 cm^{-1} was attributed to O–H stretching vibrations. Peaks at 1630 cm^{-1} were assigned to the C=C stretching of aromatic rings, indicating the presence of plant-derived polyphenols. The peak at 1750 cm^{-1} corresponds to C=O stretching, likely from lactones, ketones or carboxylic anhydrides, while the band at 1240 cm^{-1} is linked to C–C and

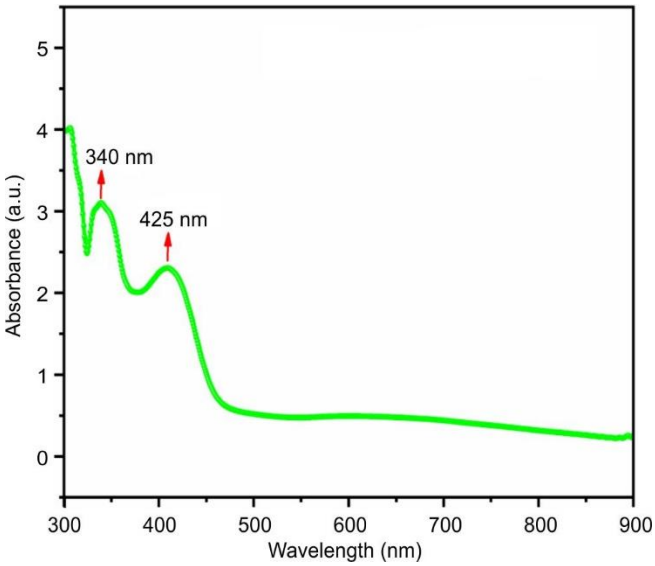

Fig. 2. UV-Vis spectra of green synthesized AgNPs

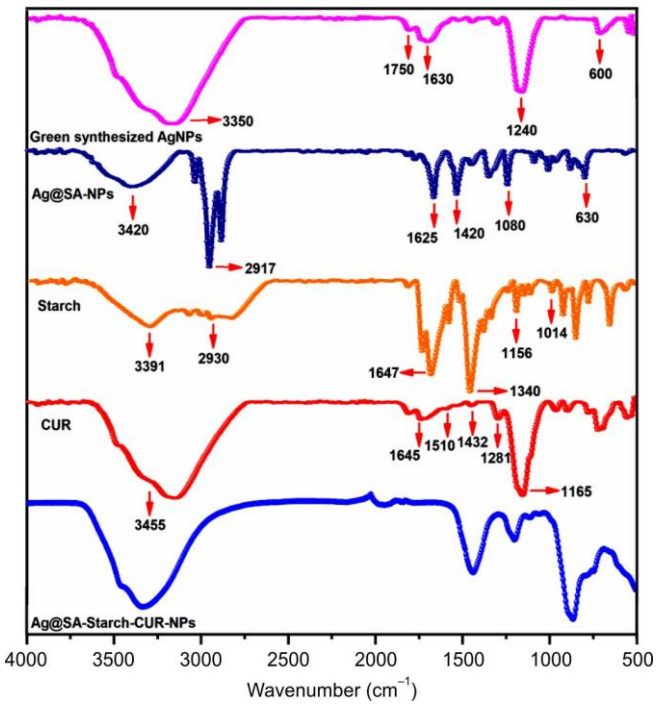

Fig. 3. FT-IR spectra of green synthesized AgNPs, Ag@SA-NPs, starch, CUR and Ag@SA-Starch-CUR-NPs

C–O stretching in phenol, ester and ether groups. A peak at 600 cm^{-1} was associated with aromatic ring stretching vibrations [32,33].

In the FT-IR spectrum of Ag@SA-NPs, the characteristic peaks at 3420 cm^{-1} correspond to O–H stretching vibrations of saponins, while C–H stretching is observed at 2917 cm^{-1}. The band at 1625 cm^{-1} indicates –COOH group vibrations. Other prominent peaks include 1420 cm^{-1} (aromatic C–C stretching), 1080 cm^{-1} (C–N stretching in aliphatic amines) and 630 cm^{-1} (=C–H bending of saponins). The starch spectrum showed a broad O–H stretching band at 3391 cm^{-1} and a band at 1647 cm^{-1} due to carboxyl groups involved in the hydrogen bonding. C–O and C–H stretching bands appeared

at 1156 cm^{-1} and 2930 cm^{-1}, respectively, with the band at 1340 cm^{-1} assigned to angular C–H deformation. Additional peaks at 1014 cm^{-1} and 1156 cm^{-1} were due to C–O stretching vibrations in alcohol and ether groups, respectively [34].

For curcumin, the FT-IR spectrum exhibited a broad band at 3455 cm^{-1} for phenolic O–H stretching. Peaks at 1645 cm^{-1} were attributed to C=O and aromatic ring stretching. The band at 1510 cm^{-1} corresponded to olefinic C–H bending attached to aromatic rings, while 1432 cm^{-1} represented C–C vibrations. The bands at 1281 cm^{-1} and 1165 cm^{-1} were assigned to C=O stretching (conjugated to aromatic rings) and C–O–C stretching, respectively [35]. The FT-IR spectrum of Ag@SA-Starch-CUR-NPs showed the characteristic peaks from AgNPs, SA, starch and CUR, confirming the successful incorporation of all components in the formation of the Ag@SA-Starch-CUR-NPs [20,21,36].

Morphology and size distribution analysis: The morphology and size of the green synthesized AgNPs were analyzed using field emission scanning electron microscopy (FE-SEM). The FE-SEM images (Fig. 4a-c) revealed that the Ag@SA-Starch-CUR-NPs predominantly possess a spherical shape with sizes ranging from 10 to 20 nm. Since FE-SEM measures the number-based size distribution, it does not account for ions and surface-bound molecules. Energy dispersive X-ray (EDX) spectroscopy (Fig. 4d) confirmed the presence of C, N, O and Ag, corresponding to components from starch and CUR. Moreover, the presence of metallic silver peaks confirms the successful incorporation of AgNPs within the nanocomposite.

Transmission electron microscopy (TEM) further elucidated the morphology and size distribution of the nanoparticles. The TEM images (Fig. 5a-c) displayed uniformly dispersed, spherical AgNPs, indicating a well-controlled synthesis process. The spherical morphology of Ag@LEC-PVA-CUR-NPs is also evident in Fig. 5d-e, suggesting efficient encapsulation within the PVA and CUR matrix. Furthermore, the adhesion of AgNPs to the nanocomposite surface implies a stable composite structure. As observed in Fig. 5f, the Ag@SA-Starch-CUR-NPs exhibited particle sizes in the range of 20-27 nm, consistent with both TEM and dynamic light scattering (DLS) analyses. These nanoscale dimensions are essential for the nanoparticles prospective biological applications.

X-ray diffraction (XRD) spectrum: The XRD spectra of green synthesized AgNPs and Ag@SA-Starch-CUR-NPs are shown in Fig. 6. The AgNPs exhibited distinct diffraction peaks at 2θ values of 20.05º, 32.17º, 42.30º, 54.22º and 57.10º, corresponding to the (110), (111), (121), (200) and (311) planes, respectively. These peaks are indicative of a pure cubic spinel crystal structure, consistent with the JCPDS card

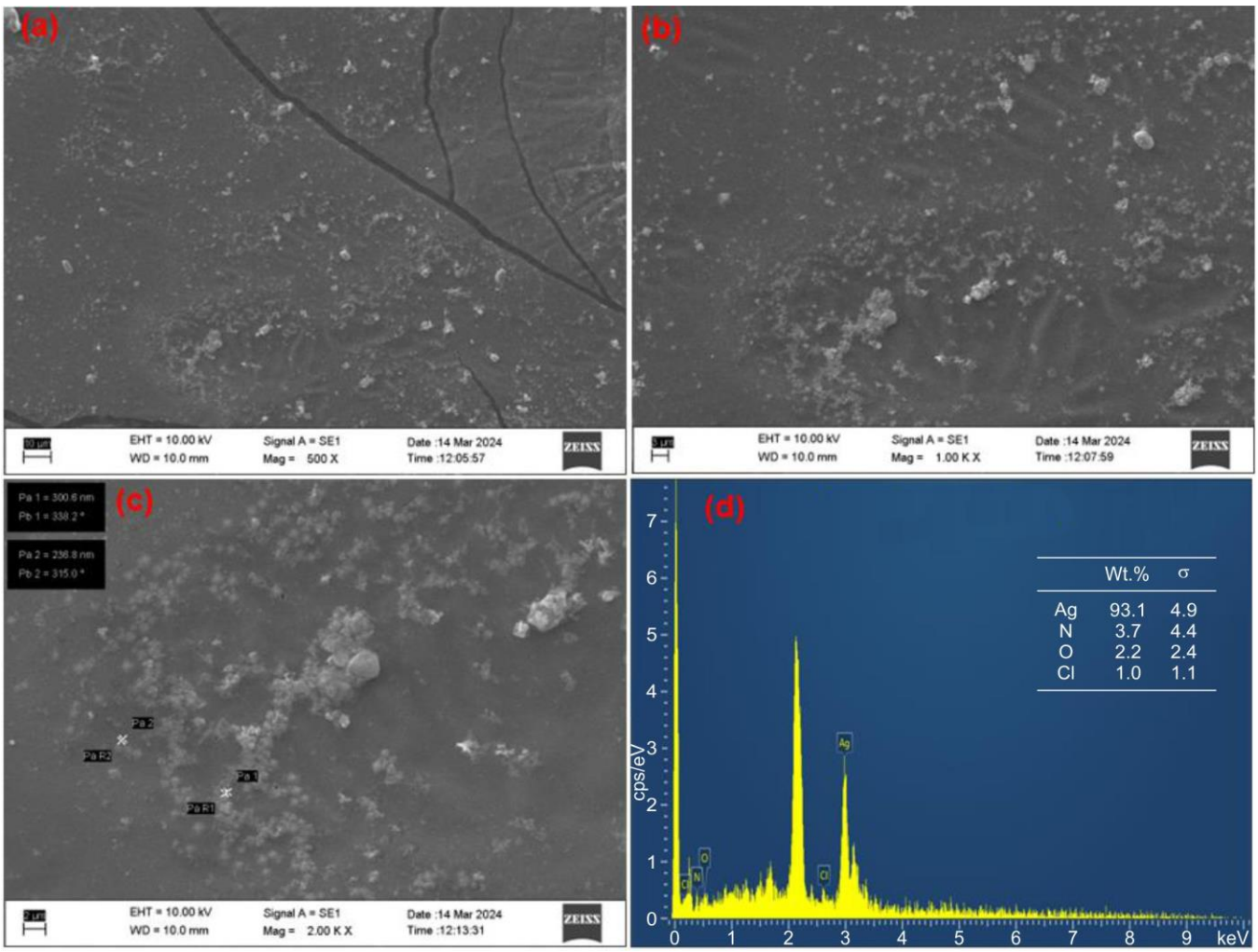

Fig. 4. (a-c) SEM image of Ag@SA-Starch-CUR-NPs and (d) EDX spectrum of Ag@SA-Starch-CUR-NPs

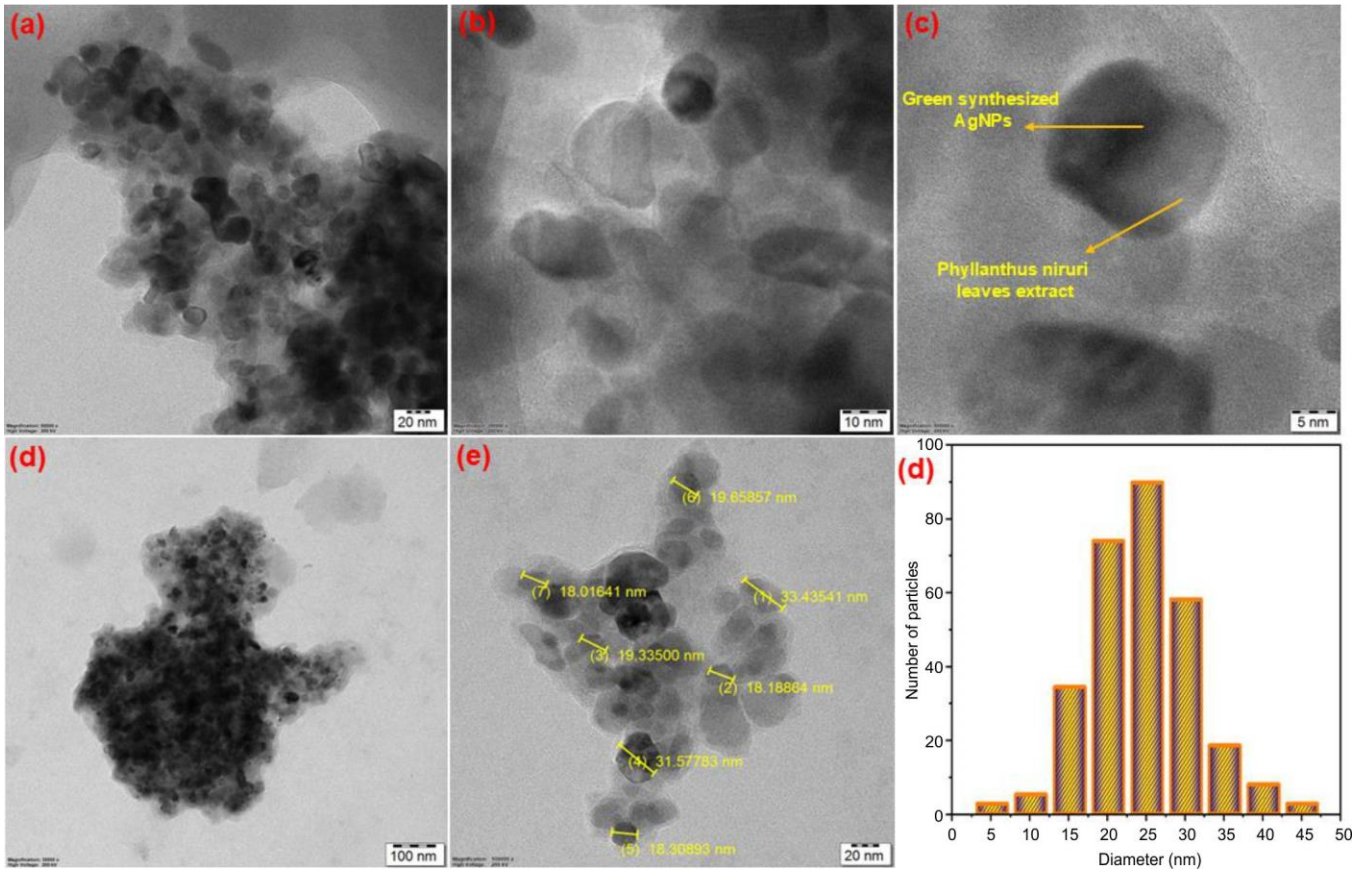

Fig. 5. (a-c) TEM image of green synthesized AgNPs (d and e) HR- image of Ag@SA-Starch-CUR-NPs (f) DLS of the Ag@SA-Starch-CUR-NPs distribution

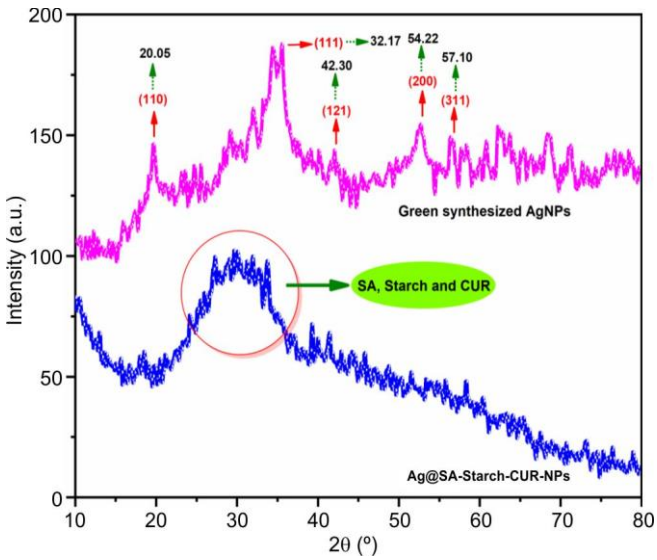

Fig. 6. XRD spectrum of the green synthesized AgNPs and Ag@SA-Starch-CUR-NPs

no. 10-041-2530 [31]. The sharp and intense peaks confirm the crystalline nature of the synthesized AgNPs. The average crystallite size was calculated using the Debye-Scherrer equation:

$$D = \frac{k\lambda}{\beta \cos\theta}$$

where $\lambda = 1.5406$ Å and $k = 0.94$, resulting in an average size of approximately 15 nm. In Ag@SA-Starch-CUR-NPs, a broad band observed between 25º-35º suggests a polycrystallline nature, likely attributed to the presence of CUR and starch. Moreover, the broadening of AgNPs peaks supports successful surface modification.

Thermal studies: Thermogravimetric analysis was employed to assess the thermal stability and composition of Ag@SA-NPs and Ag@SA-Starch-CUR-NPs (Fig. 7). Both samples displayed minor weight loss between 250-400 ºC due to the surface moisture evaporation. Ag@SA-NPs showed a significant weight loss between 600-800 ºC, leaving a residual mass of ~30.15%, corresponding to the decomposition of the saponin (SA) coating. In contrast, Ag@SA-Starch-CUR-NPs exhibited weight loss primarily between 300-450 ºC with a residual mass of ~12.20%, indicating the degradation of SA, starch and CUR components. These results suggest a reduction in thermal stability upon the incorporation of starch and CUR into the Ag@SA-NPs system.

***In vitro* drug release study:** The pH gradient along the gastrointestinal tract is a critical factor in the formulation of oral drug delivery systems, as it transitions from acidic conditions in the stomach to mildly alkaline conditions in the intestine. In this study, we investigated the release behaviour of CUR under simulated physiological conditions (37 ºC; pH 5.2 and 7.4), observing notable variations in release kinetics between these environments. As shown in Fig. 8a, the *in vitro* release

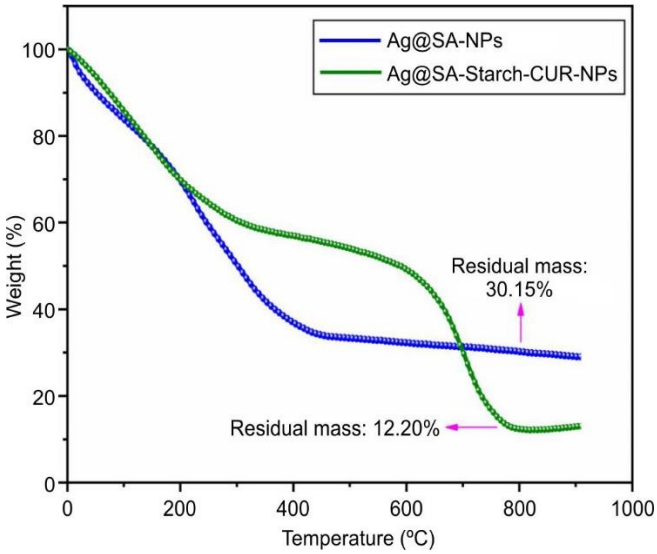

Fig. 7. Weight loss curves: for Ag@SA-NPs and Ag@SA-Starch-CUR-NPs

profile of CUR demonstrated a rapid release, with approximately 60.5% released at pH 5.2 and 44.7% at pH 7.4 within 5 h. The enhanced release at pH 5.2 is attributed to protonation-induced disruption of the hydrogen-bonded starch polymer matrix, promoting effective CUR diffusion [18,20,22]. This mechanism facilitates the extraction of CUR from the starch layer, thereby enhancing the release capacity of Ag@SA-Starch-CUR-NPs in acidic microenvironments typical of cancer cells. Interestingly, CUR exhibits heightened physiological activity under acidic conditions and demonstrates improved solubility in polar environments due to its elongated hydrophobic chain structure. Ag@SA-Starch-CUR-NPs are thus capable of withstanding the acidic gastric environment with minimal drug release, followed by a more substantial release within intestinal fluids.

To evaluate the site-specific delivery potential of Ag@SA-Starch-CUR-NPs in tumor-like conditions, CUR release was further assessed at pH 5.2 in the presence of hydrogen peroxide (H_2O_2). At physiological pH (7.4), CUR release was minimal. However, at pH 5.2, the release was significantly elevated and sustained, indicative of targeted release in cancerous tissues where acidic pH and elevated ROS levels prevail [20]. Furthermore, CUR release was studied at pH 5.2 in the presence and absence of H_2O_2 to elucidate the role of ROS in drug release modulation. As illustrated in Fig. 8b, CUR release reached 89.50% in the presence of H_2O_2 after 5 h, compared to 61.10% without H_2O_2. While CUR release at pH 5.2 alone results from the breakdown of the starch matrix, the presence of H_2O_2 also triggers cleavage of the SA layer, disrupting the interaction between its hydrophilic and hydrophobic domains. This dual-layer degradation significantly enhances the CUR release. These findings clearly demonstrated that Ag@SA-Starch-CUR-NPs exhibit pH- and ROS-responsive drug release behaviour, making them promising carriers for targeted CUR delivery to tumor sites, while minimizing the premature release into systemic circulation. Furthermore, CUR release efficiency increased proportionally with the starch content incorporated into the nanoparticle matrix [18].

***In vitro* anti-inflammatory studies:** The concentration dependent anti-inflammatory properties of Ag@SA-Starch-CUR-NPs were evaluated using a spectrophotometric hemolysis inhibition assay, which measured hemoglobin absorbance at 480 nm. Comparisons were made between Ag@SA-NPs, Ag@SA-Starch-CUR-NPs and a standard anti-inflammatory drug, diclofenac. Ag@SA-Starch-CUR-NPs demonstrated significantly enhanced anti-inflammatory activity, exhibiting an IC_{50} value of 20.13 μg/mL, which was superior to that of Ag@SA-NPs (45.30 μg/mL) and diclofenac (70.10 μg/mL), as depicted in Fig. 9. These findings suggest that Ag@SA-Starch-CUR-NPs effectively stabilize human red blood cell membranes under inflammatory conditions. Thus, preliminary *in vitro* results indicate that Ag@SA-Starch-CUR-NPs hold promise as a therapeutic candidate for the treatment of inflammatory disorders, owing to their capacity to attenuate both inflammation and oxidative stress.

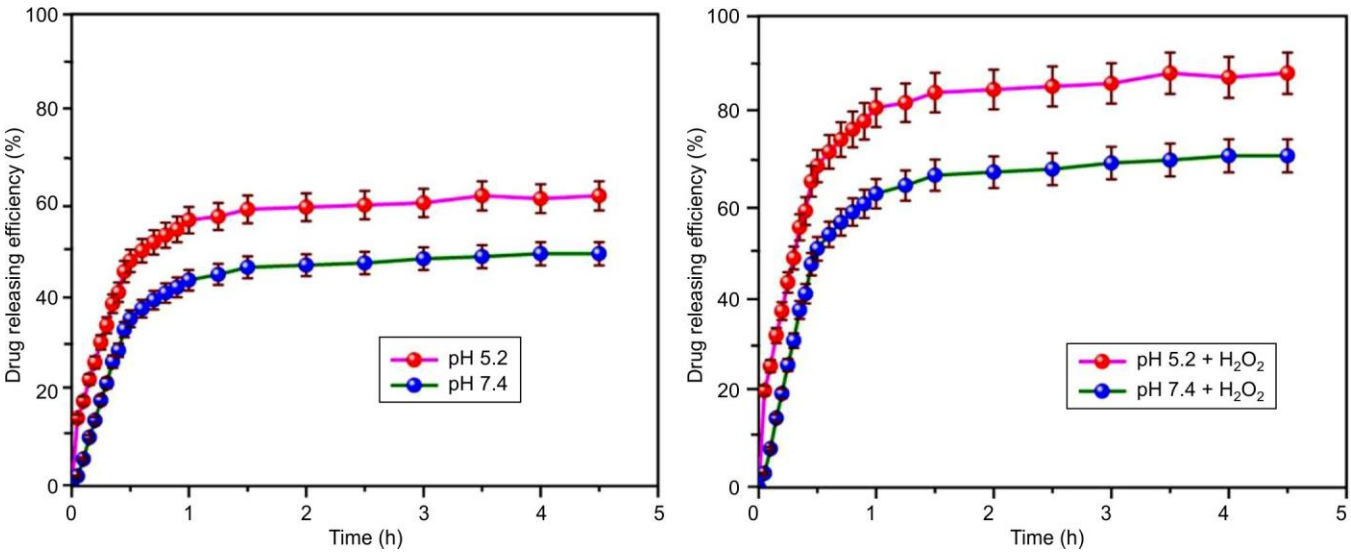

Fig. 8. (a) pH 7.4 and pH 5.2 responsive drug release curve of Ag@SA-Starch-CUR-NPs and (b) pH 7.4 and pH 5.2 + H_2O_2 (ROS)-responsive drug release curve of Ag@SA-Starch-CUR-NPs

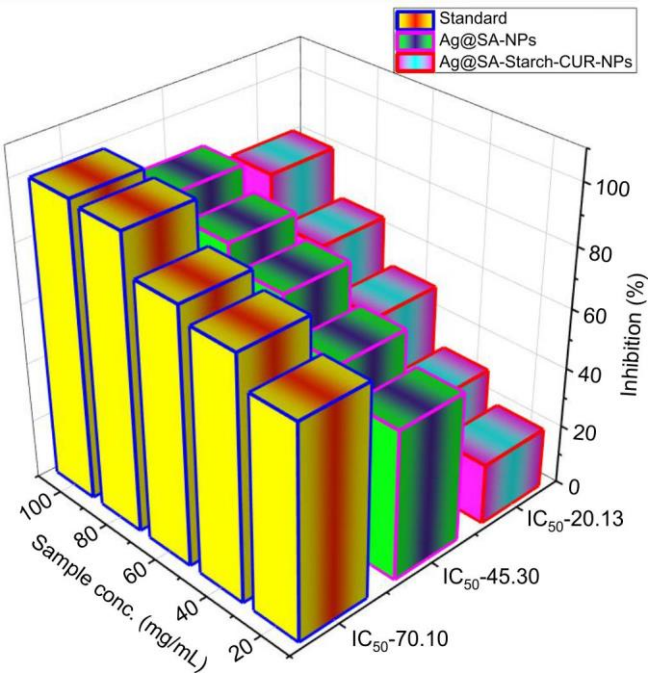

Fig. 9. *In vitro* anti-inflammatory assay data of Ag@SA-NPs and Ag@SA -Starch-CUR-NPs by HRBC membrane stabilization method

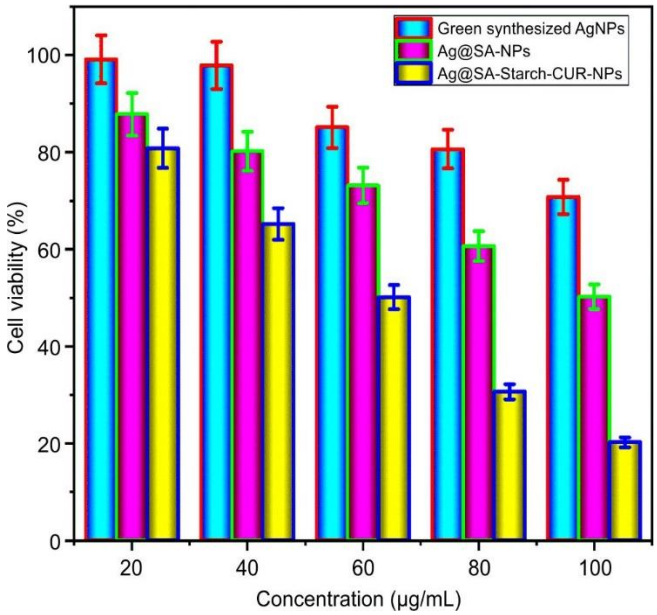

Fig. 10. The cell viability profile of MCF-7 cells treated with different concentrations (20, 40, 60, 80 and 100 µg/mL) of green synthesized AgNPs, Ag@SA-NPs and Ag@SA-Starch-CUR-NPs alone for 24 h at 37 ºC

***In vitro* cytotoxicity and morphology evaluation:** Given the enhanced anticancer drug release performance of Ag@SA-Starch-CUR-NPs, further *in vitro* cytotoxicity evaluations were conducted against MCF-7 breast cancer cell lines using the MTT assay. The cytotoxic effects, expressed as IC_{50} values, were assessed for green synthesized AgNPs, Ag@SA-NPs and Ag@SA-Starch-CUR-NPs. The nanoparticles were dissolved in DMSO and a blank solution with an equivalent volume of DMSO served as control. As shown in Fig. 10, Ag@SA-Starch-CUR-NPs exhibited the highest cytotoxic activity with an IC_{50} value of 19.5 ± 0.20 µg/mL, surpassing the cytotoxicity observed for green synthesized AgNPs and Ag@SA-NPs. This enhanced effect is likely attributed to the sustained and targeted release of CUR, enabling effective interaction with DNA base pairs and inducing apoptosis in cancer cells. Furthermore, SA known for its biocompatibility, exhibited minimal cytotoxicity toward normal human cells [37]. SA affinity for serum lipoproteins may facilitate the targeted delivery of the encapsulated drug to tumor sites. Notably, Ag@SA-NPs alone demonstrated negligible cytotoxicity against MCF-7 cells, suggesting that the observed anticancer efficacy of Ag@SA-Starch-CUR-NPs is primarily due to the curcumin payload.

The efficacy of cell death induction by green synthesized AgNPs, Ag@SA-NPs and Ag@SA-Starch-CUR-NPs was evaluated using acridine orange/ethidium bromide (AO/EB) dual staining under fluorescence microscopy. In the control group, nuclei exhibited uniform green fluorescence, indicating healthy, viable cancer cells. Treatment with 5 µg/mL of green synthesized AgNPs and Ag@SA-NPs did not induce noticeable morphological changes or fluorescence shifts, as shown in Fig. 11. In contrast, cells treated with Ag@SA-Starch-CUR-NPs exhibited prominent apoptotic features, including yellowish-orange fluorescence due to nuclear fragmentation. This result highlights the enhanced therapeutic potential of Ag@SA-Starch-CUR-NPs as an effective anticancer drug delivery system.

Conclusion

This study successfully demonstrated the green synthesis of AgNPs using a biogenic approach with *Phyllanthus niruri* leaf extract, which served as both a reducing and capping agent. The synthesized AgNPs were subsequently integrated into a ROS-responsive matrix composed of saponin (SA), starch and CUR to form Ag@SA-Starch-CUR-NPs, aimed at targeted drug delivery applications. The incorporation of these components enhanced the colloidal stability of the nanoparticles and enabled pH- and ROS-triggered controlled drug release under simulated cancer microenvironment conditions. The green synthesized AgNPs, Ag@SA-NPs and Ag@SA-Starch-CUR-NPs were successfully fabricated and thoroughly characterized using various spectroscopic and microscopic techniques. *In vitro* evaluations confirmed the multifunctional therapeutic potential of Ag@SA-Starch-CUR-NPs, revealing significant anti-inflammatory activity that surpassed that of the standard drug, diclofenac. Moreover, the nanocomposite exhibited potent anticancer activity against various cancer cell lines, highlighting its promise as an effective chemotherapeutic platform. Overall, the findings underscore the potential of Ag@SA-Starch-CUR-NPs in biomedical applications, particularly in targeted drug delivery and cancer therapy. Future *in vivo* studies and the formulation optimization are essential to fully realize their clinical translational potential.

ACKNOWLEDGEMENTS

One of the authors, K. Parvathi, express sincere gratitude to the Principal, L.R.G. Government Arts College for Women, Tiruppur for their continuous support and encouragement of research work.

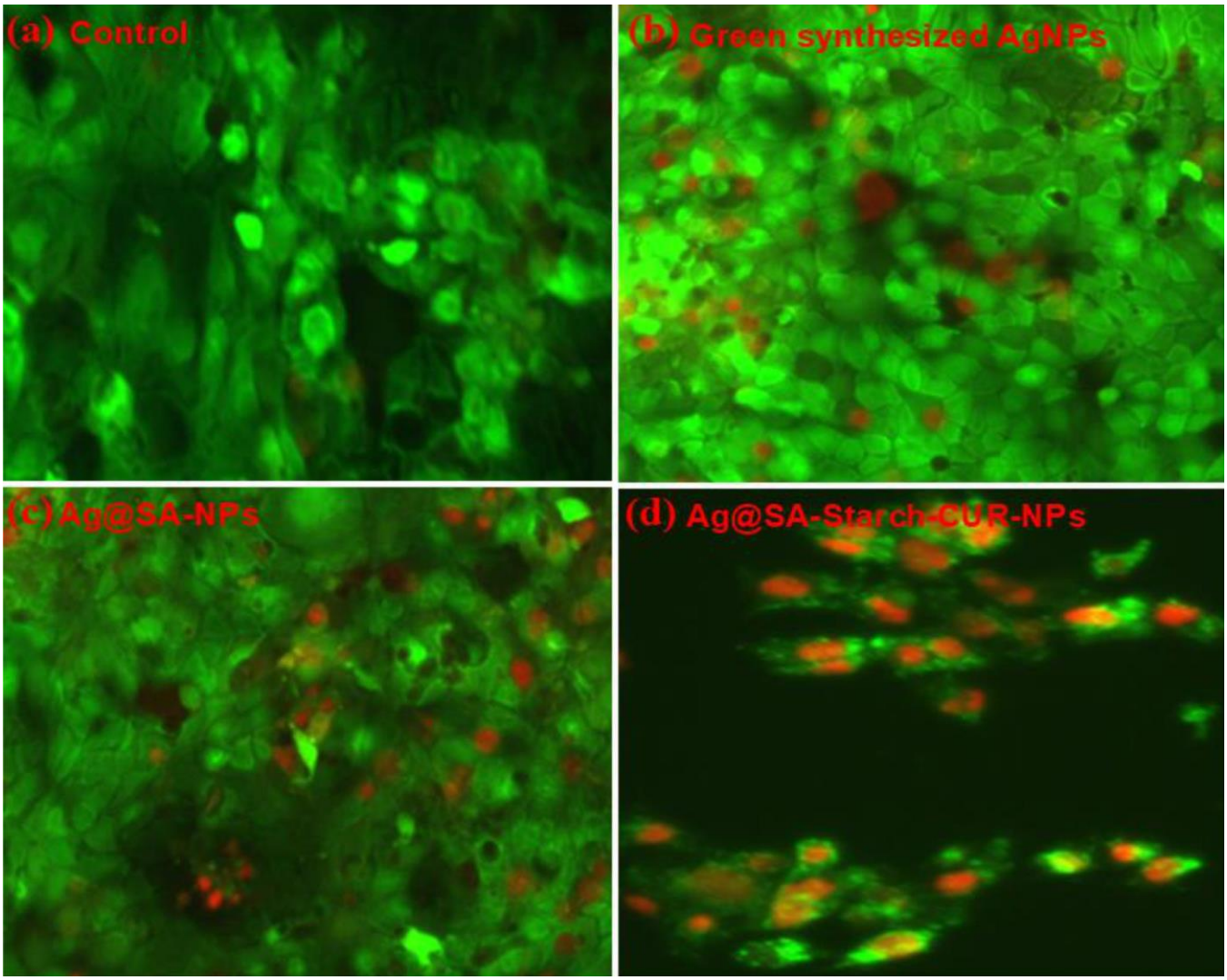

Fig. 11. (a) Fluorescence images of AO/EB stained MCF-7 cancer cells (control) treated with 5 µg/mL of (b) green synthesized AgNPs (c) Ag@SA-NPs and (d) Ag@SA-Starch-CUR-NPs

CONFLICT OF INTEREST

The authors declare that there is no conflict of interests regarding the publication of this article.

REFERENCES

1. D. Trachootham, J. Alexandre and P. Huang, *Nat. Rev. Drug Discov.*, **8**, 579 (2009); https://doi.org/10.1038/nrd2803
2. K. Brieger, S. Schiavone, F.J. Miller Jr. and K.-H. Krause, *Swiss Med. Wkly.*, **142**, w13659 (2012); https://doi.org/10.4414/smw.2012.13659
3. P.T. Schumacker, *Cancer Cell*, **27**, 156 (2015); https://doi.org/10.1016/j.ccell.2015.01.007
4. C.-C. Song, F.-S. Du and Z.-C. Li, *J. Mater. Chem. B Mater. Biol. Med.*, **2**, 3413 (2014); https://doi.org/10.1039/C3TB21725F
5. R. Fang, H. Xu, W. Cao, L. Yang and X. Zhang, *Polym. Chem.*, **6**, 2817 (2015); https://doi.org/10.1039/C5PY00050E
6. M.K.Y. Soliman, S.S. Salem, M. Abu-Elghait and M.S. Azab, *Appl. Biochem. Biotechnol.*, **195**, 1158 (2023); https://doi.org/10.1007/s12010-022-04199-7
7. G. Martínez, M. Merinero, M. Pérez-Aranda, E.M. Pérez-Soriano, T. Ortiz, E. Villamor, B. Begines and A. Alcudia, *Materials*, **14**, 166 (2020); https://doi.org/10.3390/ma14010166
8. A. Syafiuddin, M.R. Salmiati, M.R. Salim, A.B.H. Kueh, T. Hadibarata and H. Nur, *J. Chin. Chem. Soc.*, **64**, 732 (2017); https://doi.org/10.1002/jccs.201700067
9. S. Some, I. Kumar Sen, A. Mandal, T. Aslan, Y. Ustun, E.Ş. Yilmaz, A. Katı, A. Demirbas, A.K. Mandal and I. Ocsoy, *Mater. Res. Express*, **6**, 012001 (2018); https://doi.org/10.1088/2053-1591/aae23e
10. H.R. El-Seedi, M.S. Omara, A.H. Omar, M.M. Elakshar, Y.M. Shoukhba, H. Duman, S. Karav, A.K. Rashwan, A.H. El-Seedi, H A. Altaleb, H. Gao, A. Saeed, O.A. Jefri, Z. Guo and S.A.M. Khalifa, *Bioengineering*, **11**, 1095 (2024); https://doi.org/10.3390/bioengineering11111095
11. A.I. Osman, Y. Zhang, M. Farghali, A.K. Rashwan, A.S. Eltaweil, E.M. Abd El-Monaem, I.M.A. Mohamed, M.M. Badr, I. Ihara, D.W. Rooney and P.-S. Yap, *Environ. Chem. Lett.*, **22**, 841 (2024); https://doi.org/10.1007/s10311-023-01682-3
12. D.S. Chormey, B.T. Zaman, T.B. Kustanto, S.E. Bodur, S. Bodur, Z. Tekin, O. Nejati and S. Bakırdere, *Nanoscale*, **15**, 19423 (2023); https://doi.org/10.1039/d3nr03843b
13. K. Narendra, J. Swathi, K.M. Sowjanya and A.K. Satya, *J. Pharma. Res.*, **5**, 4681 (2012).

14. X. Mao, L.-F. Wu, H.-L. Guo, W.-J. Chen, Y.-P. Cui, Q. Qi, S. Li, W.-Y. Liang, G.-H. Yang, Y.-Y. Shao, D. Zhu, G.-M. She, Y. You and L.-Z. Zhang, *Evid. Based Complement. Alternat. Med.*, **2016**, 7584952 (2016); https://doi.org/10.1155/2016/7584952
15. S. Rai, E. Acharya-Siwakoti, A. Kafle, H.P. Devkota and A. Bhattarai, *Sci*, **3**, 44 (2021); https://doi.org/10.3390/sci3040044
16. Y. Liao, Z. Li, Q. Zhou, M. Sheng, Q. Qu, Y. Shi, J. Yang, L. Lv, X. Dai and X. Shi, *Int. J. Pharm.*, **603**, 120709 (2021); https://doi.org/10.1016/j.ijpharm.2021.120709
17. P.B. Lokole, G.G. Byamungu, P.K. Mutwale, N.K. Ngombe, M.K. Mpuza, V. Mudogo, R.W.M. Krause and C.I. Nkanga, *Next Nanotechnol.*, **7**, 100109 (2025); https://doi.org/10.1016/j.nxnano.2024.100109
18. M. Sun, X. Su, B. Ding, X. He, X. Liu, A. Yu, H. Lou and G. Zhai, *Nanomedicine*, **7**, 1085 (2012); https://doi.org/10.2217/nnm.12.80
19. B. Zheng and D.J. McClements, *Molecules*, **25**, 2791 (2020); https://doi.org/10.3390/molecules25122791
20. S.F. Chin, S.N.A. Mohd Yazid and S.C. Pang, *Int. J. Polym. Sci.*, **2014**, 340121 (2014); https://doi.org/10.1155/2014/340121
21. L. Mazzarino, C. Travelet, S. Ortega-Murillo, I. Otsuka, I. Pignot-Paintrand, E. Lemos-Senna and R. Borsali, *J. Colloid Interface Sci.*, **370**, 58 (2012); https://doi.org/10.1016/j.jcis.2011.12.063
22. Y. Pan, Z. Wu, B. Zhang, X.M. Li, R. Meng, H.Q. Chen and Z.Y. Jin, *Food Chem.*, **294**, 326 (2019); https://doi.org/10.1016/j.foodchem.2019.05.053
23. Y. Pan, X.M. Li, R. Meng and B. Zhang, *J. Agric. Food Chem.*, **68**, 623 (2020); https://doi.org/10.1021/acs.jafc.9b07350
24. Y. Iqbal, I. Ahmed, M.F. Irfa, S.A.S. Chatha, M. Zubair and A. Ullah, *Carbohydr. Polym.*, **321**, 121318 (2023); https://doi.org/10.1016/j.carbpol.2023.121318
25. H. Rostamabadi, S.R. Falsafi and S.M. Jafari, *Trends Food Sci. Technol.*, **88**, 397 (2019); https://doi.org/10.1016/j.tifs.2019.04.004
26. M.R. Mauricio, P.G. da Costa, S.K. Haraguchi, M.R. Guilherme, E.C. Muniz and A.F. Rubira, *Carbohydr. Polym.*, **115**, 715 (2015); https://doi.org/10.1016/j.carbpol.2014.07.063
27. D. Narayanan, S. Nair and D. Menon, *Int. J. Biol. Macromol.*, **74**, 575 (2015); https://doi.org/10.1016/j.ijbiomac.2014.12.012
28. J. Liu, Y. Pang, Z. Zhu, D. Wang, C. Li, W. Huang, X. Zhu and D. Yan, *Biomacromolecules*, **14**, 1627 (2013); https://doi.org/10.1021/bm4002574
29. C.R. Zhang, S.A. Aldosari, P.S. Vidyasagar, K.M. Nair and M.G. Nair, *J. Agric. Food Chem.*, **61**, 5834 (2013); https://doi.org/10.1021/jf401371v
30. M. Yusefi, K. Shameli, R.R. Ali, S.W. Pang and S.Y. Teow, *J. Mol. Struct.*, **1204**, 127539 (2020); https://doi.org/10.1016/j.molstruc.2019.127539
31. I. Johnson and H.J. Prabu, *Int. Nano Lett.*, **5**, 43 (2015); https://doi.org/10.1007/s40089-014-0136-1
32. G.O. Akalin, *BioResources*, **19**, 4396 (2024); https://doi.org/10.15376/biores.19.3.4396-4422
33. S. Pasieczna-Patkowska, M. Cichy and J. Flieger, *Molecules*, **30**, 684 (2025); https://doi.org/10.3390/molecules30030684
34. M. Adnan, A.J. Siddiqui, S.A. Ashraf, M.S. Ashraf, S.O. Alomrani, M. Alreshidi, B. Tepe, M. Sachidanandan, C. Danciu and M. Patel, *Antibiotics*, **12**, 1415 (2023); https://doi.org/10.3390/antibiotics12091415
35. A. Joly and M.S. Latha, *Orient. J. Chem.*, **35**, 715 (2019); https://doi.org/10.13005/ojc/350235
36. C. Liu, B. Xu, D.J. McClements, X. Xu, S. Cui, L. Gao, L. Zhou, L. Xiong, Q. Sun and L. Dai, *Food Chem.*, **391**, 133224 (2022); https://doi.org/10.1016/j.foodchem.2022.133224
37. I. Podolak, A. Galanty and D. Sobolewska, *Phytochem. Rev.*, **9**, 425 (2010); https://doi.org/10.1007/s11101-010-9183-z